ISSN 0454－4641

運輸省港湾技術研究所

港湾技術研究所報告

REPORT OF THE PORT AND HARBOUR RESEARCH INSTITUTE

MINISTRY OF TRANSPORT

VOL.39 NO.1 Mar.2000

NAGASE, YOKOSUKA, JAPAN

港湾技術研究所報告(REPORT OF P.H.R.I.)

第39巻　第1号 (Vol.39, No.1), 2000年3月 (Mar. 2000)

目　　次 (CONTENTS)

REPORT OF THE PORT AND
HARBOUR RESEARCH INSTITUTE
Vol.39, No.1(Mar.2000)

A Diagnostic Study on Water Bodies Connecting Two Open Seas

Mohamed ELZEIR[1)]
Hiroichi TSURUYA[2)]
Yasushi HOSOKAWA[3)]
Tadashi HIBINO[4)]

Synopsis

Transport in channels connecting two basins was studied with application to the Suez Canal and Kanmon Strait. The study was performed in three consecutive steps. In the first step, a 2DH, FE Model was applied. The findings of this step include: ① The Sommerfeld radiation open boundary condition is superior to other open boundary conditions. Many authors used it in the FDM. The current study applied it in the FEM.② Fields propagating in one basin are strongly damped inside the connecting channel and are not transmitted to the other basin. ③ The north and south reaches of the Suez Canal are separated by the Bitter Lakes in which changes propagating from one reach are absorbed and are not allowed to pass through to the other reach.

In the second step, a study on correlation between atmospheric pressure and water level in and around the connecting channel was performed. The findings of this step include: ① The correlation between atmospheric pressure and water level in and around Kanmon Strait is obvious. ② For the Suez Canal, there is a good correlation between water level variation in the south reach of the canal (represented by water level at Shalufa and Port Tawfiq) and pressure over the Indian Ocean (represented by pressure at Dar Es-Salam).

Key words : Suez Canal, Kanmon Strait, FEM, Sea level difference, Atmospheric Pressure Field

1) Visiting scientist, Environment Assessment Laboratory, Marine Environment Division.
2) Director, Marine Environment Division.
3) Chief, Environment Assessment Laboratory, Marine Environment Division.
4) Senior Researcher, Marine Environment Division
Address:3-1-1 Nagase, Yokosuka, Kanagawa 239-0826 Phone:(0468)44-5018 Fax:(0468)44-6243
e-mail:hibino@cc.phri.go.jp

港湾技術研究所報告
第39巻第1号(2000.3)

二つの海域を連結する狭窄部での流れに関する研究

Mohamed ELZEIR [1] ・鶴谷広一 [2] ・細川恭史 [3] ・日比野忠史 [4]

要　旨

二つの大きな海域を結び付けている水路は航海に果たす役割は大きく非常に重要であるものの，内部の流れは非常に複雑であり，またその調査は極めて困難である．したがって，このような水路内の流動解析は科学的な研究対象として非常に重要である．本研究では，エジプトのスエズ運河および日本の関門海峡を対象として検討を行った．解析には，利用可能な観測データと2次元有限要素法を用いた．また，本研究では時間スケールを強制外力の時間スケールによって二つの基本スケールに分割し検討を行った．一つは潮汐運動スケールの短い時間スケール，一つは大気圧変動スケールの長い時間スケールである．本研究で得られた主要な知見を以下にまとめる．

1．2つの開境界を有し移流や波動によって制御されている領域に対しては，領域内から外部へ伝播する波が境界で反射を起こさず境界を透過するように開境界の条件を定めるべきである．そこで，Blumberg and Kanta によって定式化された Sommerfeld radiation 開境界条件の有限要素形式化を行い，また，それが適切であることを示した．

2．本研究で用いた数値モデル（2 次元有限要素法）は検討するシミュレーションに対して十分適用可能であることが示されたが，流速についてはより一層の検討が必要である．

3．2つの海域を連結する幅の狭い水域は次の基本的特性を有する．一方の海域から入射した波の伝播速度と流体の移動速度は異なる．両者の差は水路内に大きな水面勾配を引き起こす．それ故，大きな水面勾配に対する直接的な応答として，水路内では大きな流速が生じ，船舶の航行に支障をきたす．この特性はスエズ運河の南側と関門海峡の内部で観察される．

4．スエズ運河内のビター湖は，水理学的に相互に依存した2つの区域にスエズ運河を分割している．

5．Kantara と Port Said における水位はアレクサンドリアの気圧に対して反比例している．このことは日比野・鶴谷が水位と気圧の間に相関関係があるとみなしたことと良く一致している．Shalufa と Port Tawfiq の水位は直接アレクサンドリアにおける気圧に比例するが，インド洋を広く覆う気圧に対しては反比例していることが期待される．他の場所における水位は気圧との明確な相関はない．

6．関門海峡付近の水位は日本海と瀬戸内海の両方を広く覆う気圧と極めて高い相関がある．

キーワード：スエズ運河，関門海峡，FEM，水位差，気圧場

1) 海洋環境部環境評価研究室　客員研究員
2) 海洋環境部　部長
3) 海洋環境部　環境評価研究室室長
4) 海洋環境部　研究官
所在地：〒239-0826　神奈川県横須賀市長瀬 3-1-1　TEL：(0468)44-5018　FAX：(0468)44-6243
e-mail：hibino@cc.phri.go.jp

CONTENTS

1. Introduction

Transport through a narrow channel connecting two basins is an important hydraulic issue because of the following reasons. First, such channels are usually important navigation routes; for example, the Suez Canal, Kanmon Strait, and the Strait of Gibraltar. Second, transport through the channel is usually complicated and influenced by many external parameters; for example, astronomical tides in the basins, and salinity, temperature and density difference between the waters of the two basins. Third, flow in such channels is usually characterised by fast currents and, sometimes, deposition and/or erosion, which necessitate special navigation precautions and continuous maintenance programs.

The Suez Canal of Egypt and Kanmon Strait of Japan are the focus of the current study. Both waterways are important navigation routes and have hydraulic issues that are common to most waterways connecting two open seas. Location of, importance of, and hydraulic issues related to both waterways will be addressed in Section 2. The study focused on understanding flow mechanism in both waterways. The analysis was performed with the aid of two basic tools: numerical model and field observations. In Section 3, the 2D, FEM model that was used in the present study will be explained. The domains under consideration have more than one open boundary. Therefore, a special precaution is paid to choosing the Open Boundary Conditions (OBC's) to guarantee numerical stability without introducing severe damping. The OBC's newly applied to the FEM are explained in Section 3. The model was used for short-term and long-term simulations. Short-term simulations were forced by astronomical tides. The results of simulation and the corresponding observations are analysed and compared for both the Suez Canal and Kanmon Strait in Section 4. Long-term simulations were forced by atmospheric pressure variation. The results of the simulations and corresponding observations are analysed and compared for both the Suez Canal and Kanmon Strait in Section 5. Section 6 contains the conclusions.

2. The Waterways

2.1 The Suez Canal

(1) Location

The Suez Canal runs north to south across the Isthmus of Suez in north-eastern Egypt. It connects the Mediterranean Sea with the Gulf of Suez, an arm of the Red Sea (**Fig. 1**). The canal is approximately 163 km long, with minimum bottom width of 60m, average depth of 20 m, and average top width of 300m. it is the longest unlocked channel in the world because the Mediterranean Sea and the Gulf of Suez have roughly the same water level and the Isthmus of Suez is a part of the flat desert of Sinai Peninsula. Excavation of the canal began on April 25, 1859, and the canal opened to navigation on November 17, 1869.

The Mediterranean Sea is a land-enclosed sea having an east to west extent of some 3860 km, and a maximum width of about 1600 km. It is generally shallow, with an average depth of 1500 m, and maximum depth of 5150 m off the south coast of Greece. An undersea ridge from Tunisia to Sicily divides the Mediterranean Sea into east and west basins. Another seafloor ridge, from Spain to Morocco, lies at the west outlet of the Mediterranean Sea. Only 300 m deep, it restricts circulation through the narrow Strait of Gibraltar, thereby greatly reducing the tidal range of the sea and coupled with high rates of evaporation, which is not compensated for by fresh water inflows, making the Mediterranean Sea much saltier than the Atlantic Ocean.

The Red Sea is a narrow, inland sea, separating the Arabian Peninsula (west Asia) from north-east Africa. It extends north-west from the Strait of Bab al-Mandab to Suez, Egypt, for a distance of about 2253 km. The maximum depth of the sea is about 2134 m, and its maximum width is about 354 km. The north extremity of the sea is divided by the Sinai Peninsula into the gulfs of Suez and Aqaba (Funk and Wagnalls

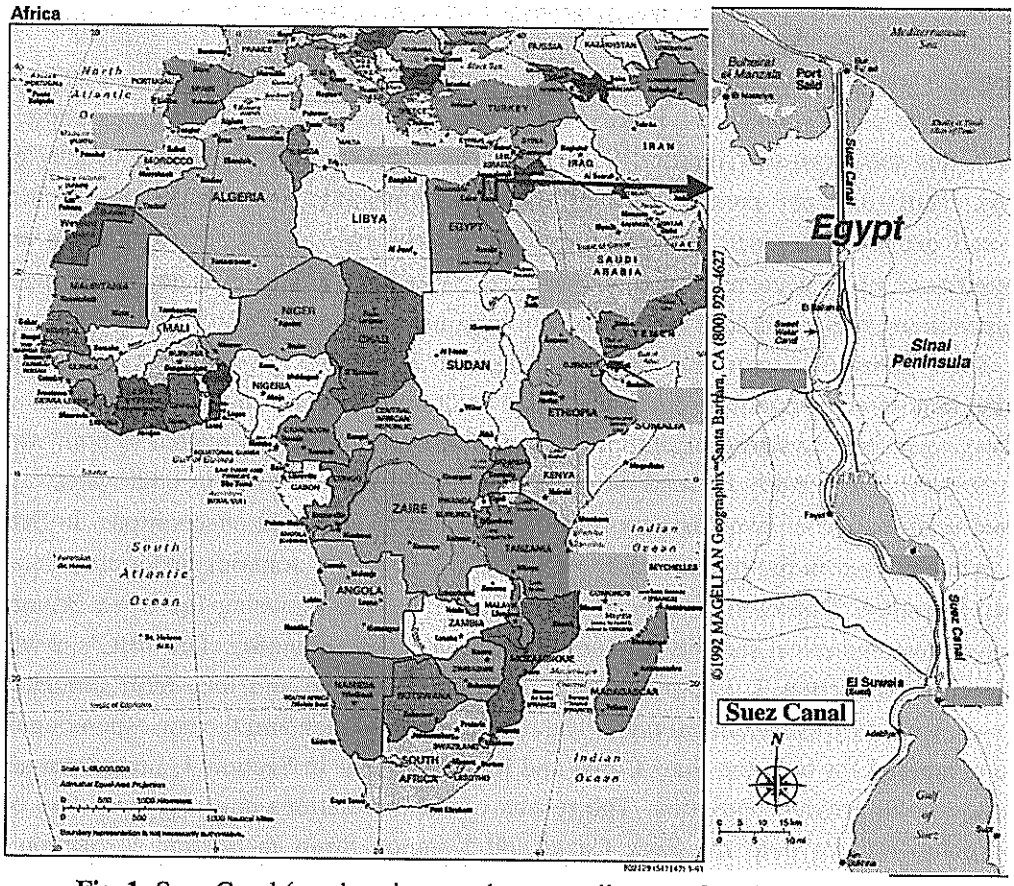

Fig. 1: Suez Canal (numbers in parentheses are distances from Port Said in km)

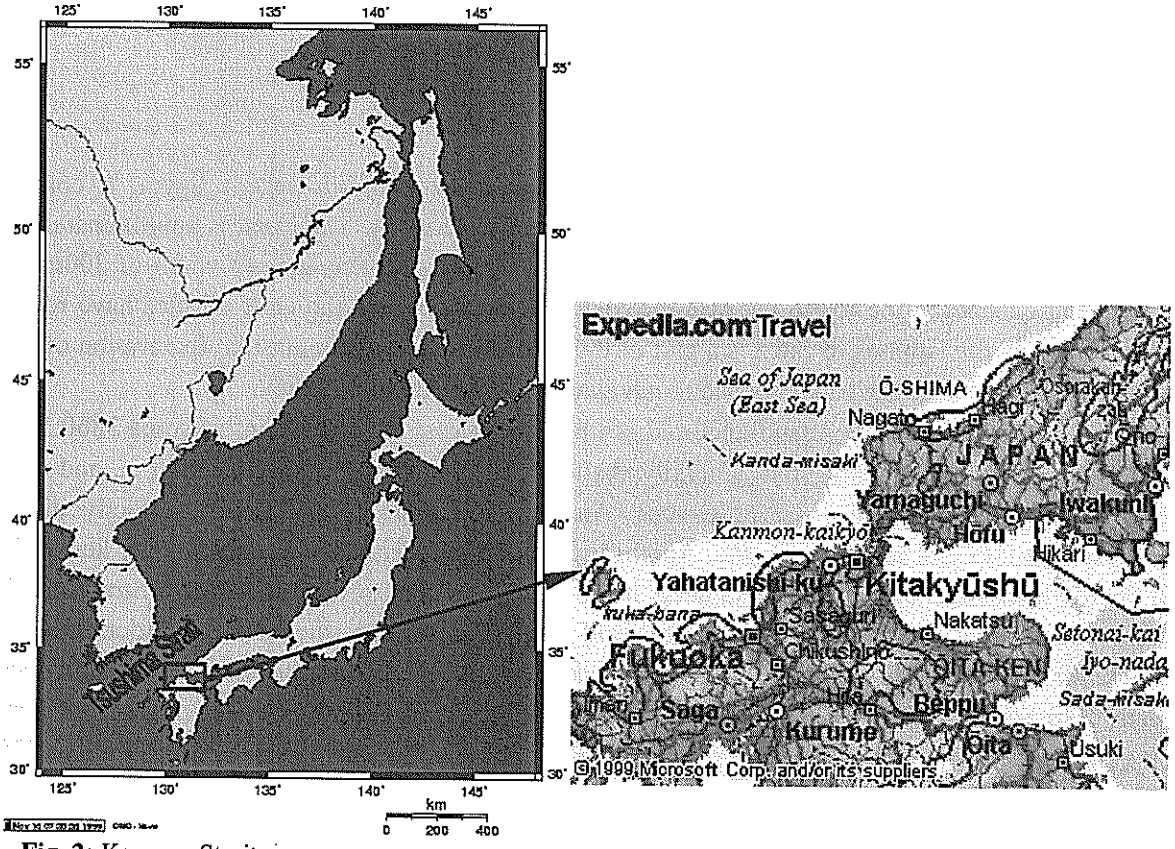

Fig. 2: Kanmon Strait

Encyclopaedia[1]).

(2) Importance

The canal makes possible a comparatively direct sea route between America and Europe on the one hand and the Far East and the Persian Gulf on the other hand. It allows ships to pass from the Mediterranean Sea to the Indian Ocean and vice versa without having to navigate around the Cape of Good Hope. Navigation in the canal is safe because the canal is straight, deep and has no locks. Therefore, the average ship transit time in the canal is only about 15 hours. Approximately, 23% of the distance between Tokyo (Japan) and Rotterdam (the Netherlands) is saved if the Suez Canal is used instead of the Cape route.

(3) Hydrodynamic Issues

The canal is characterised by two main distinct features. Firstly, at the north entrance, sediment carried by the Mediterranean waters is deposited in the canal. Therefore, the canal is permanently dredged to maintain a reasonable water depth for navigation. Secondly, average ship speed in the canal is 13 to 14 km/hr; but in the southern sector of the canal (between the Bitter Lakes and the Gulf of Suez), the speed varies between 11 and 15 km/hr. In the south sector, the ship speed is reduced when fast current prevails.

2.2 Kanmon Strait

(1) Location

Kanmon Strait, also known as Shimonoseki Strait, is an S-shaped 40-km long water passage between Shimonoseki on Honshu Island and Moji on Kyushu Island. It connects Inland Sea with Japan Sea (**Fig. 2**) (Nakazono[2])

Japan Sea is an arm of the Pacific Ocean lying between Japan on the east and the Asian mainland on the west. It is semi-closed, connected to the Sea of Okhotsk on the north by La Pérouse Strait and Tatar Strait, to the Pacific Ocean, on the east by Tsugaru Strait, to Inland Sea by Kanmon Strait, and to China Sea on the south by Tsushima Strait. The length of the sea from Tatar Strait to Tsushima Strait is about 2400 km, and its maximum width from the Japan coast to the Russian coast is about 800 km. The depth is about 2000-4000 m in the central area (Odamaki[3])

Inland Sea (in Japanese: Seto Naikai) is an arm of the Pacific Ocean in Japan. It is between Honshu Island on the north and the islands of Shikoku and Kyushu on the south. The sea is connected to the Pacific Ocean by Bungo Strait and Kii Channel. The sea is about 356 km long, 15-50 m deep and varies from 13 to 64 km wide (Funk and Wagnalls Encyclopaedia[1]).

(2) Importance

Studies concerned with Japan Sea (Odamaki[3]) and Inland Sea (Murakami et al.[4] and Hayakawa et al.[5]) do not take Kanmon Strait into account because it has negligible role in the hydrodynamic characteristics of both seas. Nevertheless, the importance of the strait arises from its vital role for ships en-route between the important Japanese ports of Yokohama and Kobe and East Asia, South East Asia, and Europe via the ports of Shimonoseki, Kita Kyushu, and Hakata. It, also, serves significant domestic shipping within Japan. About 50% of sea-traffic between Japan and Korea goes through Kanmon Strait. The other alternative is Kagoshima offshore route south to Kyushu, which is 8 hours longer than Kanmon Strait one. On average 800 ships cross the strait every day (Nakazono[2]).

(3) Hydrodynamic Issues

The strait faces three main difficulties. First, the basic formation of the strait is hard rock. Therefore, expansion plans are costly. Out of 16 water routes around Japan, Kanmon Strait consumed 80% of their total construction budget allocated for the five-year plan (1991-95). Second, the strait is narrow. The number and size of ships crossing the strait increases; but plans to widen and deepen the navigation channel are hindered by the difficulty encountered in digging the rocky bed. Third, water current at many places along the strait gets fast. In

Hayatomo Seto (near Shimonoseki), a current speed of 8 knotes (4 m/s) was reported, and in front of Tobatake, a current speed of 12 knotes (6 m/s) was reported. Such a high speed poses threat to navigating units, especially large containers. It also hinders construction works.

3. Numerical Model

3.1 Governing Equations

The governing equations of shallow water flow are:

$$\frac{\partial U_i}{\partial t} + U_j U_{i,j} + g\zeta_{,i} + \frac{\tau_i^b}{\rho(h+\zeta)} - A_l(U_{i,j} + U_{j,i})_{,j} + f_i = 0 \tag{1}$$

$$\frac{\partial \zeta}{\partial t} + [(h+\zeta)U_j]_{,j} = 0 \tag{2}$$

where $\boldsymbol{U}$ is the mean horizontal velocity, ζ is the water elevation, h is the mean water depth, g is the gravitational acceleration, A_l is the eddy viscosity and $\boldsymbol{f}$ is Coriolis force. The bottom friction, τ, is determined as

$$\tau_i^b = \frac{n^2 g}{h^{1/3}} U_i (U_k U_k)^{1/2} \tag{3}$$

where n is the Manning coefficient.

In this report, the standard index notation and the summation convention with repeated indices are employed. The governing equations mentioned above are based on the following assumptions:

1. Navier-Stokes equations are integrated over the depth assuming hydrostatic pressure distribution.
2. The Reynolds stresses together with the viscosity term are modelled by a constant eddy-viscosity term.

3.2 Finite Element Formulation

The finite element scheme developed by Kashiyama et al.[6), 7)] was applied in the present study. The scheme has the following characteristics.

1. The mesh consists of linear triangular elements.
2. The bottom friction term is linearized.
3. For discretization in time, the three-step explicit time integration scheme is used.
4. Kashiyama et al.[6), 7)] applied the selective lumping scheme introduced by Kawahara et al.[8)]. It was argued that the selective lumping scheme combines the advantages of the consistent formulation, which does not damp the numerical solution but produces spatial oscillations, with that of the lumped formulation, which produces no oscillations through the introduction of excessive diffusive effects; and therefore, may smear the results. In the present study, it was found that it is not only the consistent formulation that is responsible for the oscillating results but the OBC formulation as well. Therefore, the consistent formulation, as opposed to the selective lumping one, was adopted in the present study with special attention being paid to the OBC formulation, as explained in Subsection 3.3

3.3 Boundary Conditions

Numerical models of finite domains, as a part of the infinite real world domain, inevitably involve the treatment of boundaries where the numerical grid ends. Boundaries, generally, fall into one of two categories: solid boundaries and open boundaries. Solid boundaries are real physical boundaries. They are, generally,

easily dealt with, except perhaps for movable boundaries, for example, those used in modelling flooding and drying (Lorenzzetti and Wang[9]). On the other hand, open boundaries are imaginary boundaries, where the numerical domain ends but the physical processes do not end. Therefore, the interaction between the limited numerical domain and the outside world should be known. As the numerical behaviour of the environment of the region outside the computational domain cannot be known, some kind of extrapolation of knowledge obtained in the interior of the domain must be used. The specification of the OBC depends on, among others, the character of the equation to be solved; hyperbolic, parabolic or elliptic (Orlanski[10]). For flow problems dominated by advection and/or wave motion, the OBC should be transparent; that is, they should allow propagating waves, which are generated within the computational domain to pass through with minimum reflection and/or distortion. There is no universal OBC that achieves this condition (Chapman[11]). Consequently, it has been suggested that using approximate "*ad hoc*" OBC may be the most reasonable approach to the problem at this time (Bennett and McIntosh[12]).

An OBC that is applied extensively in the finite element models (Kashiyama et al.[6], Kawahara et al.[8], Koutitas and O'Conner[13]) is stated as

$$U_n = \zeta^I \frac{g}{\sqrt{gh}} \tag{4}$$

where U_n is the mean velocity over depth normal to the open boundary, ζ^I is the incident wave height, and $\sqrt{gh}$ is the surface gravity wave speed. Kodama et al.[14] criticised Eq. 4 as it does not allow outgoing waves to be transmitted through the open boundary. Both Kodama et al.[14] and Elzeir and Hibino[15] proposed similar remedies. They divided wave height at the open boundary, ζ, into two parts: incident wave height, ζ^I, and reflected wave height, ζ^R. Kodama et al.[14), 16] determined the reflected wave height and velocity assuming that it is produced only by astronomical force and relating it to the height and velocity of the waves at the interior nodes. Elzeir and Hibino[15] argued that the formulation of Kodama et al.[14), 16] has two disadvantages. First, the incident wave is determined using only empirical equations and constants for astronomical tides. Second, nodes near the open boundaries are manipulated during estimating the open boundaries. Hence, they are affected by the open boundary treatment in a similar way to that of the sponge layer OBC where significant number of grid points close to the open boundary are wasted. Elzeir and Hibino[15] overcame both disadvantages by considering the numerical wave (numerical error) as the difference between calculated and observed water levels at the nodes located immediately on the open boundary; and therefore, by using values at the open boundary nodes instead of some interior nodes. All the above-mentioned suggestions have a common disadvantage: the velocity at the open boundary is directly proportional to water level.

Another approach to the OBC treatment was proposed by Elzeir and Hibino[15]. They introduced the Sommerfeld radiation condition:

$$\varphi_{,t} + C\varphi_{,n} = 0 \tag{5}$$

where φ is the variable to be defined at the open boundary (either U or ζ) and C is the phase speed (or advection velocity). They mentioned that the Sommerfeld condition was successfully applied in the finite difference schemes while finite element modellers have been wary of applying it for fear of difficulty. Elzeir and Hibino[15] could apply the Sommerfeld condition in finite element scheme using the formulation proposed by Blumberg and Kanta[17] in their finite difference model (POM). Blumberg and Kanta[17] took C equal to the local, flat bottom, shallow water, surface gravity wave spped:

$$C = \sqrt{gh} \tag{6}$$

and added an "*ad hoc*" friction-like term $(\frac{-\varphi}{T_f})$ on the right hand side of Eq.5, where T_f is a friction time scale. T_f

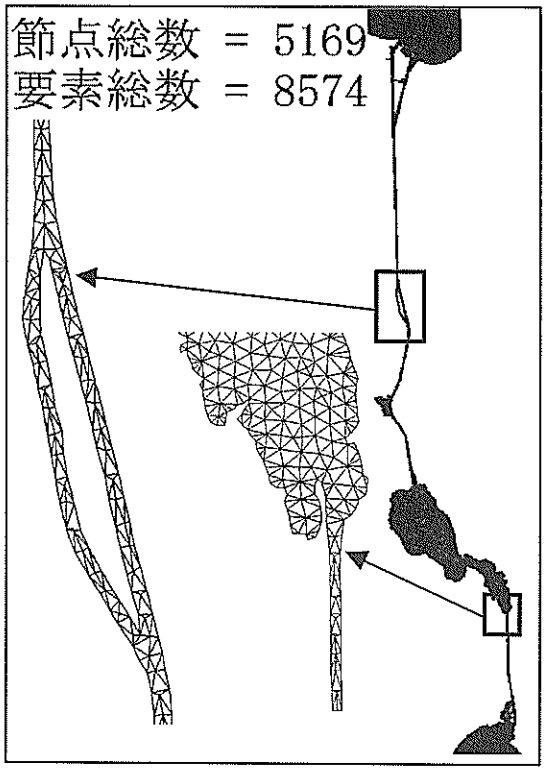

Fig. 3: Computational domain of the Suez Canal

is estimated by numerical experiment. In applying the radiation OBC, Elzeir and Hibino[15] defined a boundary element as that finite element which has at least one of its *sides* coincides with the open boundary. Later, Elzeir et al.[18] refined the definition to be: a boundary element is that finite element which has at least one of its *nodes* coincides with the open boundary. The later definition improved the performance of the radiation OBC. The OBC formulated by Elzeir et al.[18] was used in the present study.

4. Astronomical Tide Effect

4.1 Suez Canal

The calculation domain was discretised into 5169 nodes and 8574 elements (**Fig. 3**). The following values were used for simulation. A_l = 10 m^2/s, n=0.04, and latitude (for Coriolis term) = 30° 30` N. The available observations are water level monitoring at Port Said, Kantara, Geniva, and Shalufa during 6 months (from January to June, 1997). Observations were recorded every 30 minutes. As there are no available observations at the (Red and Mediterranean Seas) open boundaries, the OBC's were estimated using a numerical experiment. The numerical experiment has two objectives:

1. to estimate suitable values for the friction time scale (T_f)
2. to extrapolate the available observations to the open boundaries.

The forcing tide in the numerical experiment was described by the following equation

$$\zeta = A \sin \omega t \qquad (7)$$

where A is the wave amplitude (1.5 m) and ω is the wave frequency ($\frac{2\pi \text{ radians}}{12 \text{ hours}}$). The computation was carried out until a quasi-steady state was obtained. Tidal forcing was applied at both open boundaries to estimate T_f for velocity. Tidal forcing was applied at only one open boundary and water level is estimated using radiation OBC at the other open boundary to estimate T_f for elevation. It was noticed that results at the Red Sea open boundary

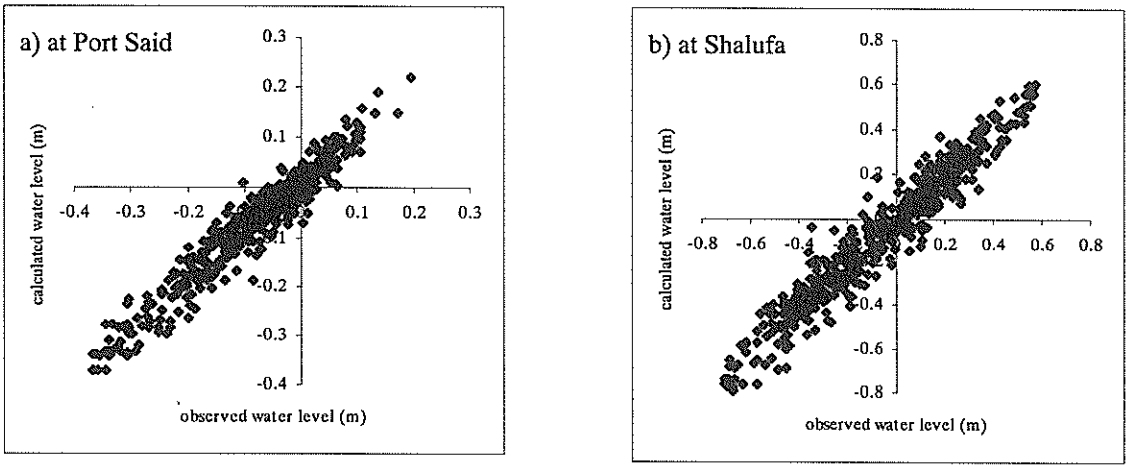

Fig. 4: Correlation between observed and calculated water levels

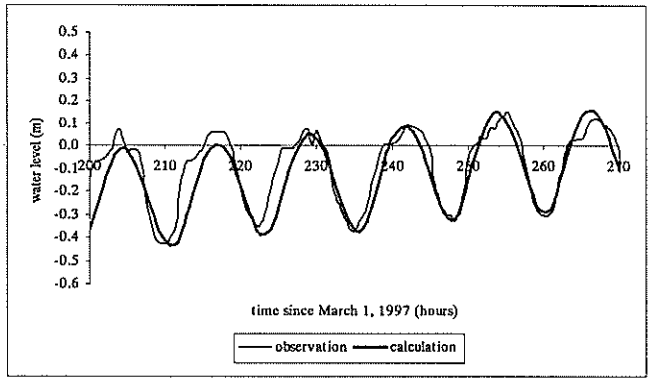

Fig. 5: Comparison between observed and calculated water levels at Geniva

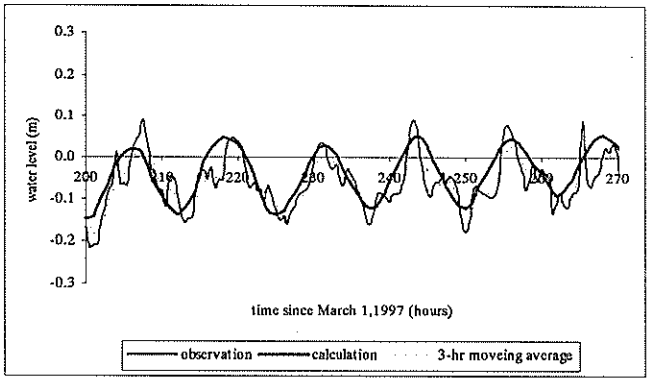

Fig. 6: Comparison between observed and calculated water levels at Kantara

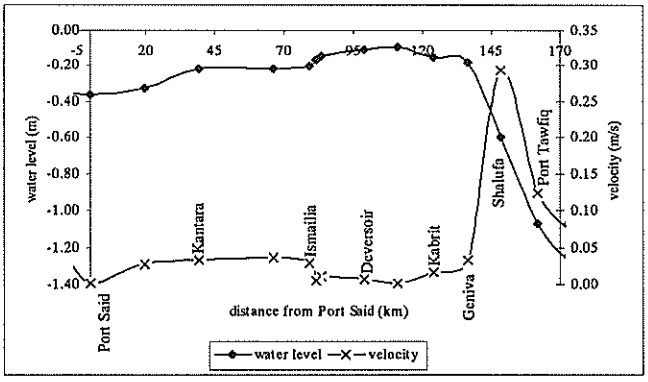

a) Tidal forcing at both open boundaries, LWL.

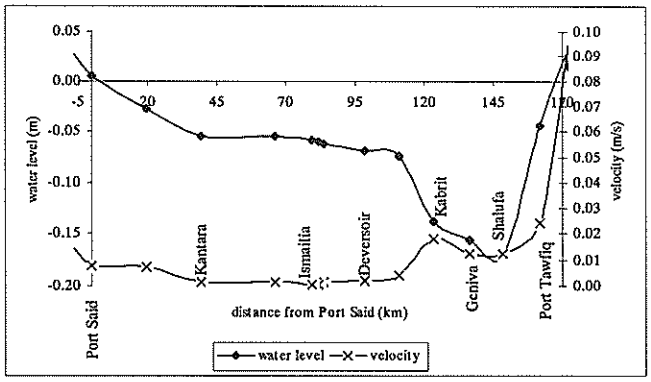

b) Tidal forcing at both open boundaries, MWL.

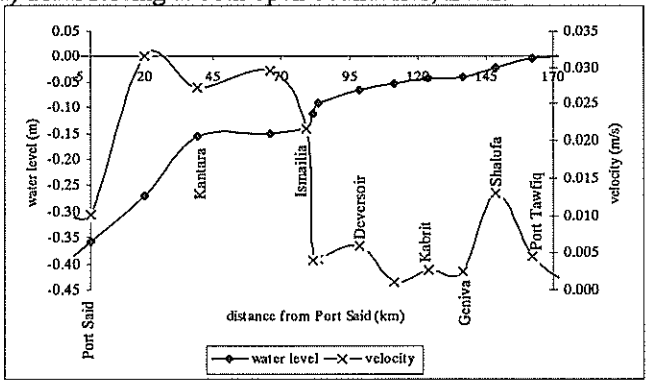

c) Tidal forcing at Mediterranean Sea only, LWL.

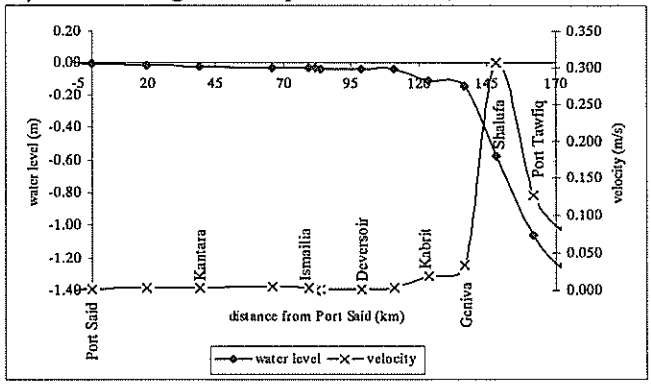

d) Tidal forcing at Red Sea only, LWL.

Fig. 7: water surface and velocity profiles along the Suez Canal

are very sensitive to T_f and Δt values. This sensitivity was attributed to both shallow and steep topography. The wave amplitude at Port Said is 84.3% of that applied at the Mediterranean Sea open boundary with a lag of 32 minutes. The wave amplitude at Shalufa is 52.8% of that applied at the Red Sea open boundary with a lag of 34 minutes. T_f values are summarised in **Table 1.**

Table 1 T_f values for the Suez Canal open boundaries

Run	velocity		elevation		Δt
	T_f at Red Sea	T_f at Med. Sea	T_f at Red Sea	T_f at Med. Sea	(sec)
Forcing at both open boundaries	5.80	5.90			5.0
Forcing at Red Sea only				5.00	5.0
Forcing at Mediterranean Sea only			5.60		4.0

Conclusions obtained from the real-world simulation are discussed in the following paragraphs (**Fig. 4 – Fig.7**).

1. Observed and calculated water levels are in good agreement at both Shalufa and Port Said (**Fig. 4**). However, water level observations at both stations were used to estimate OBC's.
2. Comparing observed and calculated water levels at Geniva (**Fig. 5**), it is clear that both are in phase. However, the positive wave amplitudes are not perfectly matching each other while the negative ones are in good agreement. Moreover, the negative amplitude is about 35 cm and the positive amplitude is about 12 cm, referred to a common datum for the whole canal. Also, the observed tide has a gradually changing gradient in the negative part while in the positive part, the gradient is abruptly changing. The gauges used for observation are the well-and-float type gauges (**photo 1**). It is expected that the float's upward movement be sometimes hindered causing the above-mentioned water-level recording anomaly.
3. Comparing calculated and observed water levels at Kantara (**Fig. 6**), it is clear that each observed wave has two consecutive peaks of the same sign and some oscillations although the flow in the canal is (relatively) slowly changing. This phenomenon is not observed at any other station. Using (3-hour) moving average of the observations, the oscillations disappeared and it becomes clear that there is a phase lag between observation and calculation. The observed peak lags about 90 minutes behind the calculated peak.
4. From the longitudinal profiles (**Fig. 7**), it is clear that water in the Great Bitter Lake is almost stagnant. The strong damping effect is attributed to the wide shallow water body of the lake that intercepts the narrow (relatively) deep canal. Thus, the propagating waves are absorbed inside the lake.
5. From **Fig. 7a,** the maximum velocity occurs in the south reach of the canal. Its value is about 0.4 m/s. Unfortunately, there is no velocity measurements to compare with. However, the position of maximum calculated velocity is in good agreement with reported comments obtained from the Suez Canal Authority. Current in the south reach of the canal is faster than currents elsewhere along the canal because the water level gradient in the south reach of the canal is steeper than that in the rest of the canal. The steep gradient in the south reach of the canal is produced due partly to the proximity between the Bitter Lakes, where waves are almost damped, and the Red Sea. Another reason for the steep gradient is that the tidal amplitude in the Gulf of Suez (about 1.3 m) is approximately twice as large as that in the Mediterranean Sea (about 0.5 m). Amplitudes in the open seas are quoted from Eid et al.[19].

4.2 Kanmon Strait

The calculation domain is discretized into 10764 nodes and 20274 elements (**Fig. 8**). The time step was 10 seconds for all runs. The following values were used for simulation. A_l = 10 m^2/s, n=0.04, and latitude (for Coriolis term) = 33° 50` N. A numerical experiment similar to that used in Subsection 4.1 was carried out to estimate T_f and choose suitable stations for estimating OBC's. It was noticed that numerical results are sensitive

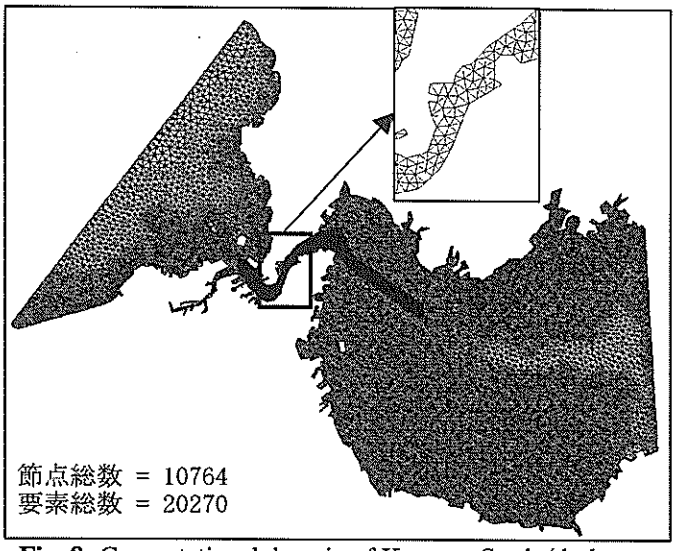

Fig. 8: Computational domain of Kanmon Strait (dark part indicates the navigation channel)

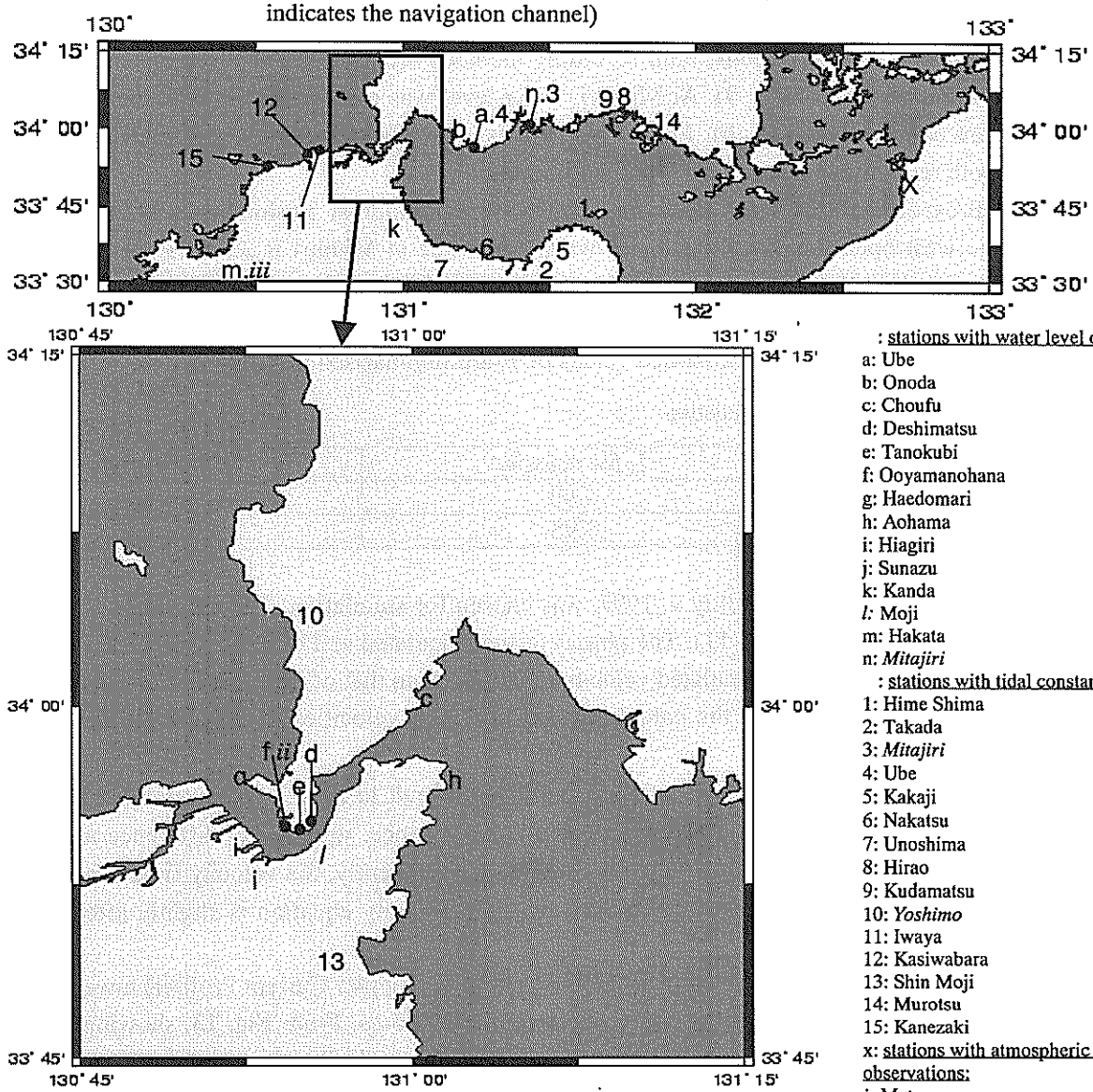

: stations with water level observation:
a: Ube
b: Onoda
c: Choufu
d: Deshimatsu
e: Tanokubi
f: Ooyamanohana
g: Haedomari
h: Aohama
i: Hiagiri
j: Sunazu
k: Kanda
l: Moji
m: Hakata
n: *Mitajiri*

: stations with tidal constants:
1: Hime Shima
2: Takada
3: *Mitajiri*
4: Ube
5: Kakaji
6: Nakatsu
7: Unoshima
8: Hirao
9: Kudamatsu
10: *Yoshimo*
11: Iwaya
12: Kasiwabara
13: Shin Moji
14: Murotsu
15: Kanezaki

x: stations with atmospheric pressure observations:
i: Matsuyama
ii: Shimonoseki
iii: Fukuoka

Fig. 9: Stations with available data at and around Kanmon Strait. : water level observations, : tidal constants, x: atmospheric pressure observations.

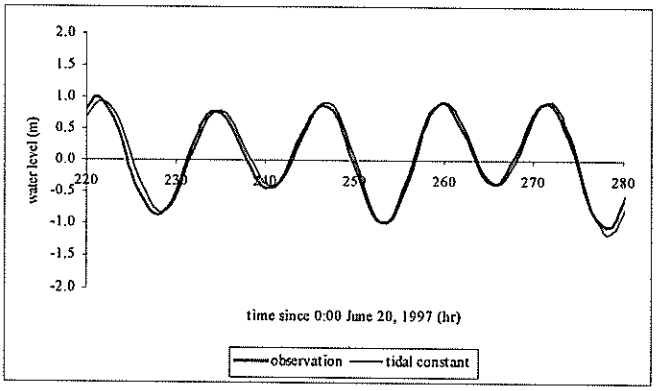

Fig. 10: Water level records at Mitajiri

to variation of T_f at the west open boundary (Japan Sea), where bathymetry is similar to the Red Sea area in the Suez Canal simulation, steep and shallow.

Water level records at and around Kanmon Strait are available from either observations or estimations using tables of tidal constants. At some stations, both recording methods are available while at other stations, only one recording method is available (**Fig. 9**). At Mitajiri, water level was recorded using both methods. Records by both methods are compared in **Fig. 10**. From **Fig. 10** it is clear that records by both methods are almost identical. Hence, both records can be used for OBC's estimation.

From the numerical experiment results, it was found that wave amplitude at Yoshimo is 1.3% larger than the wave applied at the west open boundary. Also, the wave amplitude at Mitajiri is 3.5% larger than the wave applied at the east open boundary. Phase lag is 2.6 minutes and 21 minutes, respectively. Hence, tidal wave estimated at Yoshimo from tidal constants and that observed at Mitajiri were used to estimate OBC's at west and east open boundaries, respectively. Calibrated values of T_f are summarised in **Table 2.**

Table 2: Calibrated T_f for Kanmon Strait simulation

	T_f for velocity	T_f for elevation
East open boundary	5.60	5.60
West open boundary	5.95	5.30

A 22-day period, from June 18, 1997 to July 9, 1997, was chosen for simulation. The calculated and observed water levels are in good agreement (**Fig. 11**). The phases of the calculated and observed velocities are in good agreement while the magnitude of the calculated velocity is smaller than that of the observed one (**Fig. 12**). The discrepancy between the magnitudes of the calculated and observed velocities is expected to be due to the following reasons.

1. Because Japan is always subjected to seismic effects, it is difficult to have a fixed reference that can be used constantly, in terms of both time and space, as a datum. Hence, water level difference and gradient applied between open boundaries do not match the reality. Consequently, the velocity field is significantly affected. On the other hand, water level determined by the continuity equation is slightly affected by the water level gradient.
2. Velocity observations were performed using an ADCP (Acoustic Doppler Current Profiler) towed by a ship, which scanned cross sections of the strait every one hour for 25 hours. From **Fig. 13**, showing locuses of the ship, it can be seen that the ship does not follow exactly a single line representing a cross section. Rather, it moves within an area. Therefore, velocity interpolation among the available data contains some error.

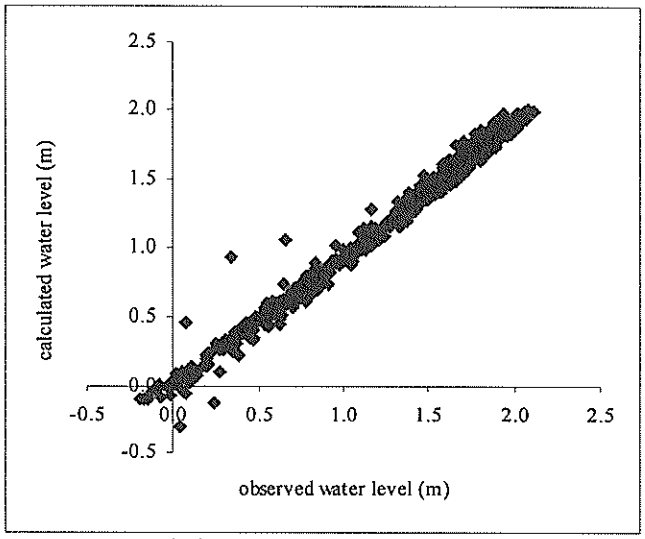

Fig. 11: Correlation between observed and calculated water levels at Moji.

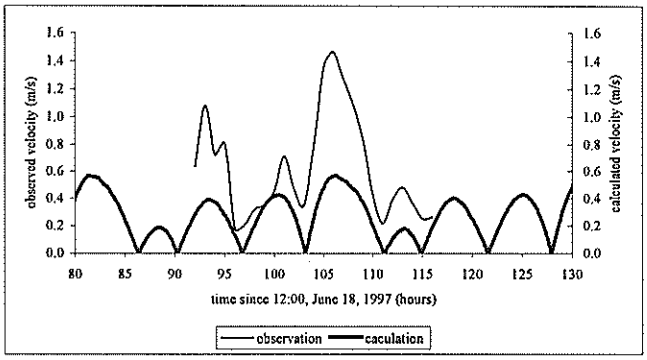

Fig. 12: Comparison between observed and calculated velocities in the navigation channel at Moji.

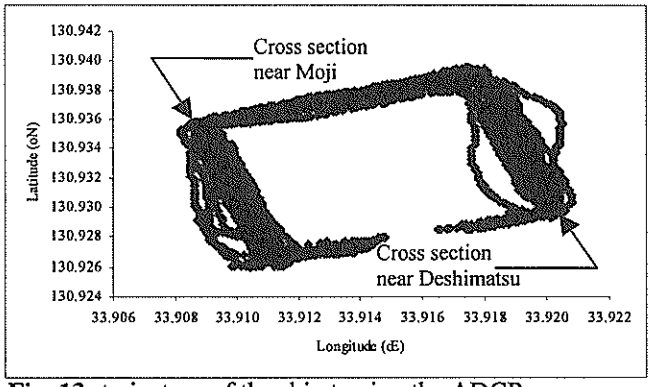

Fig. 13: trajectory of the ship towing the ADCP.

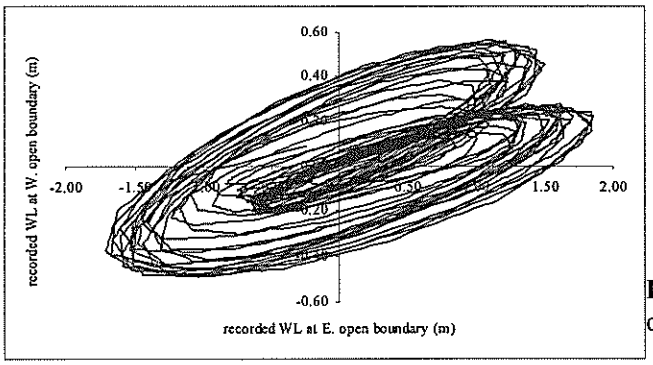

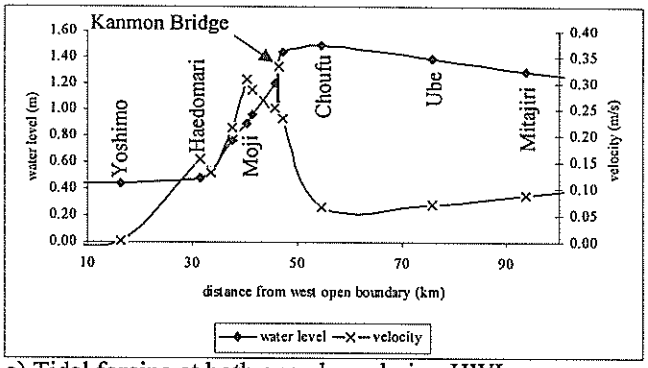

a) Tidal forcing at both open boundaries, HWL.

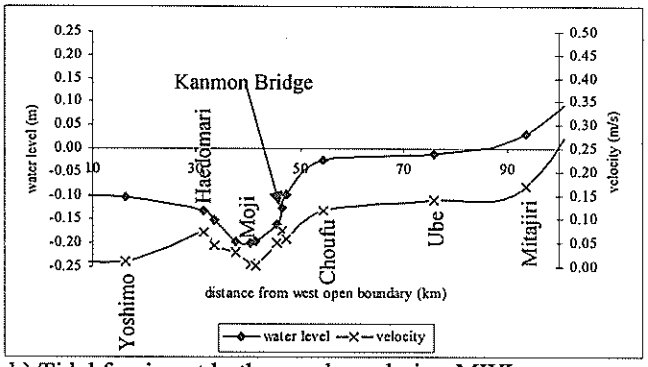

b) Tidal forcing at both open boundaries, MWL.

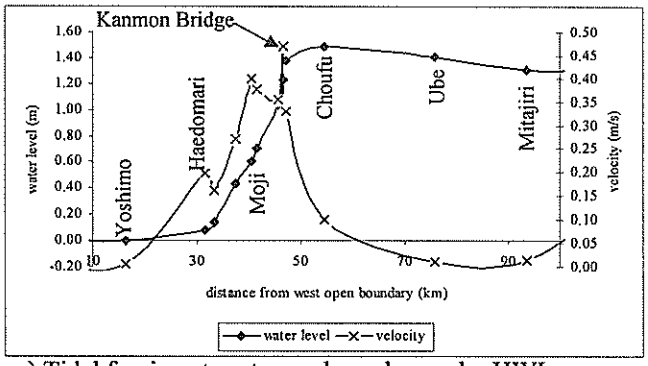

c) Tidal forcing at east open boundary only, HWL.

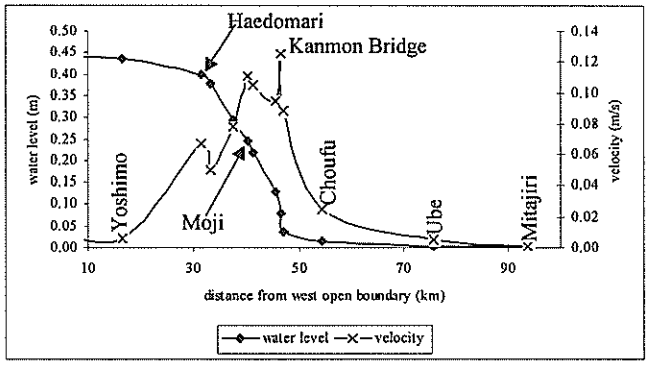

d) Tidal forcing at west open boundary only, HWL.

Fig. 14: Water surface and velocity profiles along Kanmon Strait.

Fig. 15: Comparison between tides at east and west open boundaries of Kanmon Strait.

From **Fig. 14**, the following can be noticed. A wave propagating inside the strait from one open sea is gradually damped inside the strait so that it is completely dissipated and does not have any effect on the other open sea. The damping is attributed to the large water body on the other end of the strait not to the narrowness of the strait itself. When the water level is close to MWL, the velocity is minimum. Its maximum value occurs at Moji (**Fig. 14 b**). when the water level is different from MWL, the velocity increases. There is a sharp increase of the velocity at the narrowest part of the strait (at Kanmon Bridge).

Comparing tides at east and west open boundaries (**Fig. 15**), there is a phase lag between tides of both seas. The phase lag during neap tide is different from that during spring tide. Tidal amplitude in Japan Sea is about 0.60 m and that in Seto Inland Sea is about 1.8 m.. Thus, the tidal difference is about 1.0 m.. The length of the strait (from Haedomari to Aohama) is about 23 km.. Hence, there is a great similarity between Kanmon Strait and the south reach of the Suez Canal (about 1.3 m tidal difference and 25 km length). Geometrically, both courses are narrow, (relatively) short channels connecting two large water bodies. The south reach of the Suez Canal is shallower than the Red Sea but deeper than the Bitter Lakes while Kanmon Strait is shallower than both Japan and Seto Inland Seas. Hibino et al.[20] performed a similar study. The domain, they investigated, consists of three water bodies (**Fig. 16**): Niho Bay, Lake Nakaumi , and Lake Shinji connected by narrow short channels. Lake Shinji and Niho Bay have large surface areas as compared with Lake Nakaumi and the connecting channels. The three domains (Suez Canal, Kanmon Strait, and MNS) have the following in common:

1. two water bodies of large surface areas connected by narrow passage.
2. Wave propagating from one body with large surface area is damped in the other water body. The damping produces water-surface gradient change inside the connecting passage. Velocity inside the connecting passage increases due to the water-surface gradient.

The north reach of the Suez Canal has different hydrodynamic characteristics because it has different geometry. The north reach of the canal is long, connecting the Mediterranean Sea and the Bitter Lakes. Also, there are bypasses and small lakes (e.g. Temsah Lake) along the north reach of the canal.

5. Atmospheric Pressure Effect

5.1 Annually water variation of Suez Canal

The monthly averaged data for the years 1995-96 and the annually averaged data for the years 1980-96 at 8 stations were analysed. The stations are (**Fig. 1**): Port Said, Kantara, Ismailia (Temsah Lake), Deversoir, Kabrit, Geniva, Shalufa, and Port Tawfiq. From the analysis, the following is concluded.

1. Water level at Deversoir (north inlet of the Bitter Lakes) and Temsah Lake are always lower than that at Port Said and Kantara. However, water level at Kantara exceeds that at Port Saif from October to January and vice versa during the rest of the year (**Fig. 17 a**).
2. Water level at Port Tawfiq is always higher than that in the Bitter Lakes (Geniva, Kabrit, and Deversoir). However, water level at Shalufa becomes lower than that at Geniva from November to April (**Fig. 17 b**). hence, there is a continuous net inflow from the Red Sea into the canal, and water stored in the Bitter Lakes from April to November is released during the rest of the year.
3. Water levels at Deversoir and Kabrit are the lowest all over the year. Hence there is no net flow exchange between the two parts of the canal through the Great Bitter Lake. A similar conclusion was drawn from the analysis of tidal effects (**Subsection 4.1**, point number 4).
4. From the annual averaged water levels (**Fig. 18**), it is clear that the water level at Port Tawfiq is always higher than that of Geniva, Kabrit, and Deversoir. Hence, there is a net inflow from the Red Sea into the canal, which is stored in the Bitter Lakes. There must be a sink to maintain continuity in the canal. The annual average of the water level at Kantara is always higher than that at Port Said. Hence, there is a net

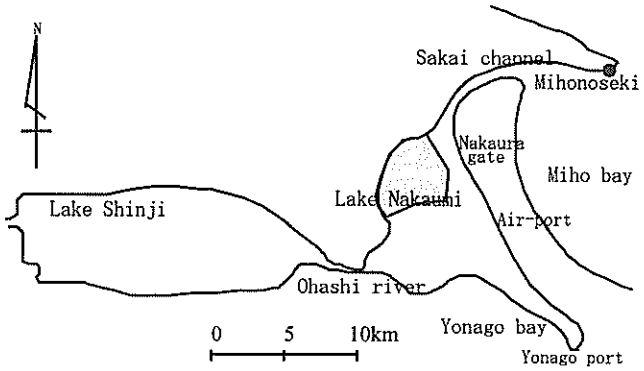

Fig. 16: Domain studied by Hibino et al.[20].

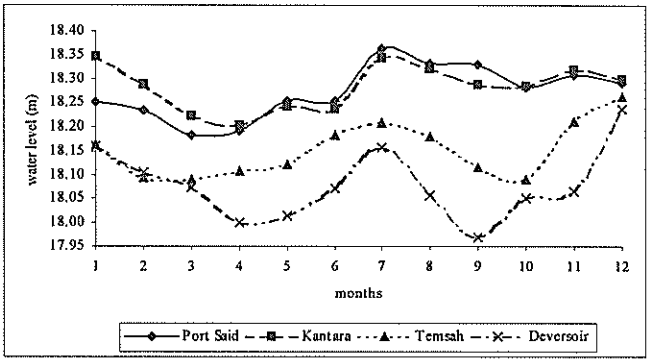

a) along the north reach

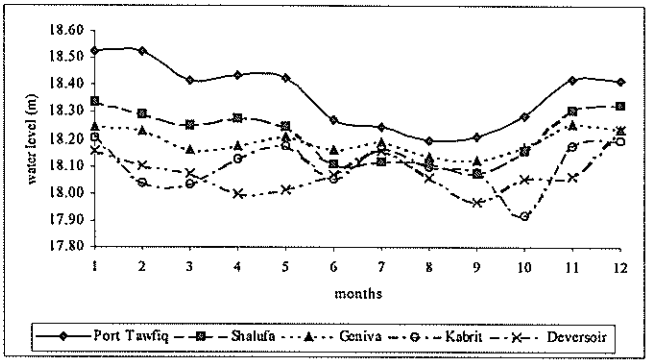

b) along the south reach

Fig. 17: monthly-averaged MWL in the Suez Canal (average of 1995 and 1996)

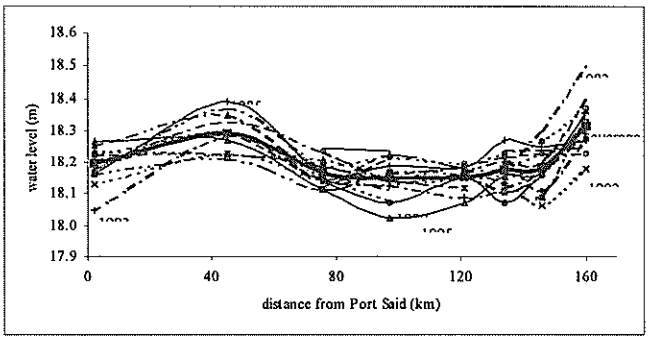

Fig. 18: annual-averaged water level along the Suez Canal

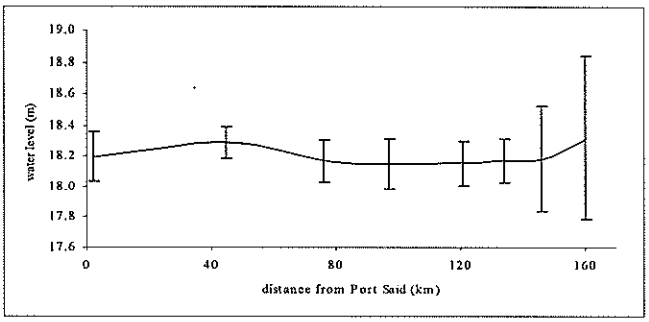

Fig. 19: MWL and tidal range along the Suez Canal (annual average)

outflow from Kantara into the Mediterranean, that outflow must be compensated by a source to maintain continuity in the canal.

5. From **Fig. 19**, the tidal range in the Red Sea is large. It decreases towards the Bitter Lakes, increases again between Bitter and Temsah Lakes, and decreases between Temsah Lake and the Mediterranean Sea. Thus, Temsah and Bitter Lakes divide the canal into three sections. The behaviour of the south section is that explained in **Section 4** for narrow channels connecting two open seas. The other two sections need further investigtions.

5.2 Correlation between atmospheric pressure distribution and sea level

Hibino and Tsuruya[21] explained that there is a strong correlation between atmospheric pressure distribution and sea level. They put the following relation as a rule-of-thumb:

Distinct seasonal patterns can be observed for the meteorology of Japan. During summer the Ogasawara high pressure system develops over the Pacific Ocean. In winter season, the Siberian high pressure system develops over the Asian continent. As the Siberian high pressure system is the highest one in the world, the atmospheric

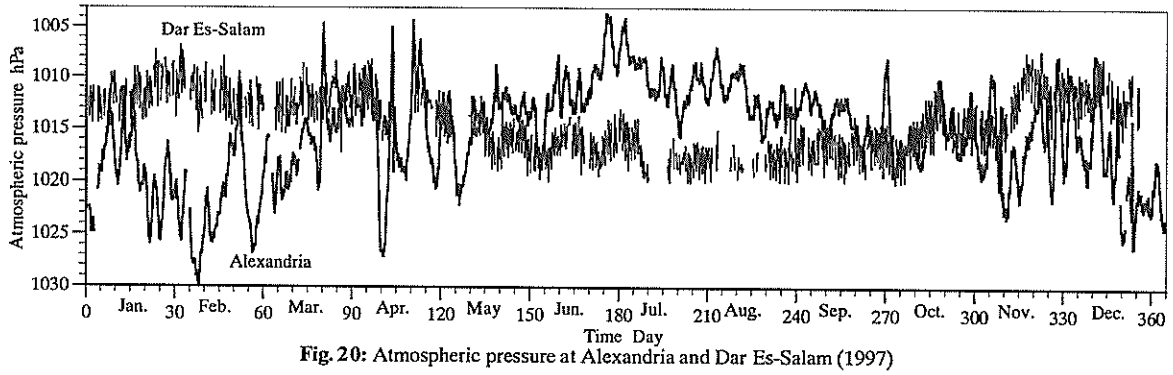

Fig. 20: Atmospheric pressure at Alexandria and Dar Es-Salam (1997)

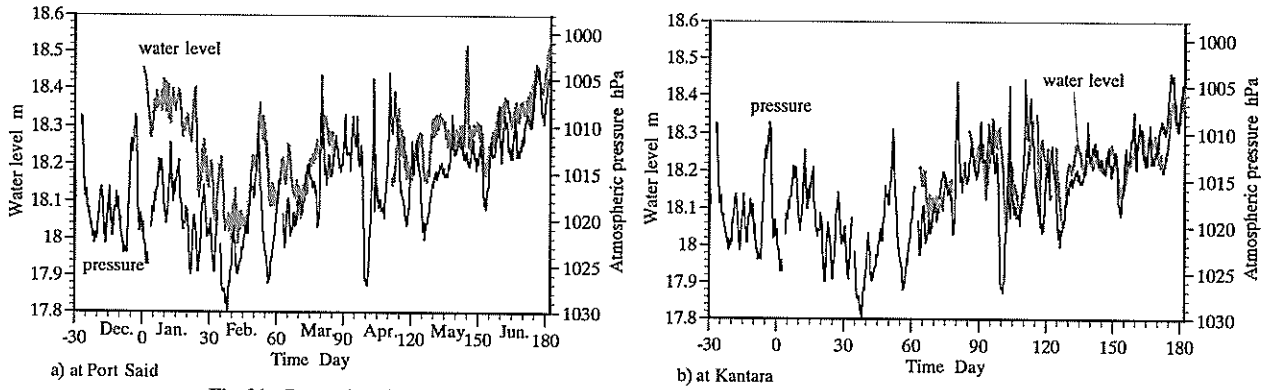

Fig. 21: Comparison between water level and pressure (Alexandria) in the north reach of Suez Canal (1997)

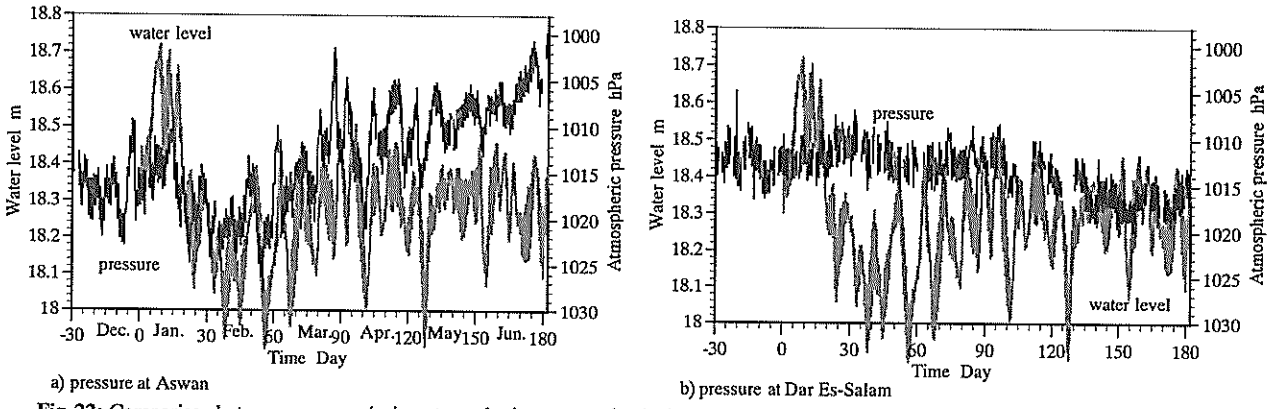

Fig. 22: Comparison between pressure (using atmospheric pressure forcing) and water level (Shalufa) in the south reach of the canal (1997)

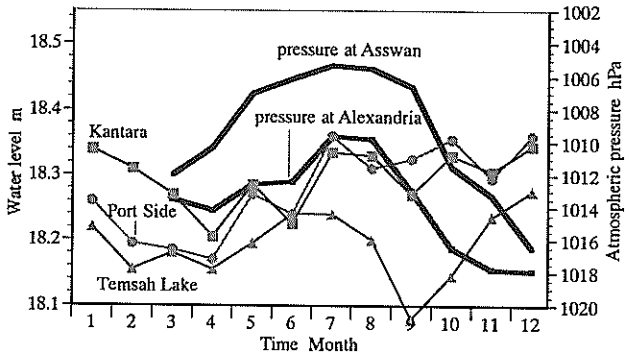

Fig. 23: Correlation between atmospheric pressure at Alexandria and water levels at Port Said and Kantara (1996)

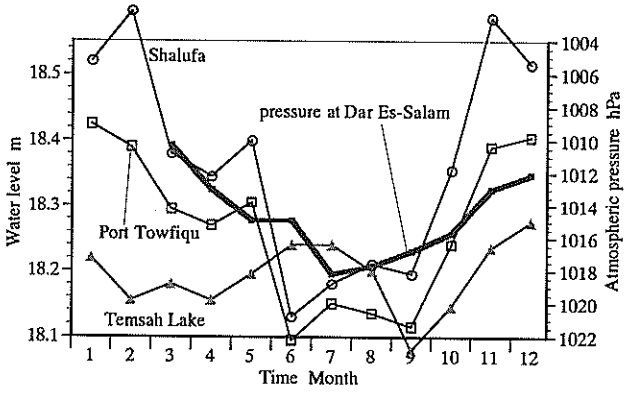

Fig. 24: Correlation between atmospheric pressure at Dar Es-Salam and water levels at Temsah Lake, Shalufa and Port Tawfiq (1996)

pressure along the coast of Japan is higher in winter than in summer. With this variation of pressure arrangement, the sea level along the coast starts to rise in spring and starts to descend in Autumn. This increase (decrease) of 1 hPa of atmospheric pressure causes a fall (rise) of 2.5 cm of seawater-level.

Considering the Suez Canal, the prevailing pressure pattern in the canal area is that prevailing on the Mediterranean Sea, represented by pressure distribution at Alexandria or Asswan, Egypt (**Fig.A-1**). Over the Indian Ocean, represented by pressure distribution at Dar Es-Salam in Tanzania, distinct seasonal pressure pattern was observed (**Fig.20**).

The forcing at the Mediterranean Sea was estimated as the atmospheric pressure variation at Alexandria for the first half of 1997 (**Fig. 21**). The results show a good agreement between water level and pressure at both Port Said and Kantara. The water level at Shalufa (the south reach of the canal) and the pressure at Asswan (similar variation with pressure at Alexandria) had good agreement till April, however, from May, the seawater level fallen as the pressure at Asswan decrease (**Fig. 22** a)). From May, the water level at Shalufa was similar variation with the pressure at Dar Es-Salam (**Fig. 22** b)). From May to August, the pressure at Alexandria become lower than at Dar Es-Salam in Tanzania (**Fig.20**). Hence, the water levels in the south reach of the canal were influenced by a force difference from the atmospheric pressure of the Suez Canal area. The influencing force is inversely proportional to that exerted by the pressure in the Suez Canal area. Investigating pressure distribution, it was found that pressure on the Indian Ocean, represented by that at Dar Es-Salam (Tanzania), was opposite to that in the Suez Canal area (**Fig. 20**). Consequently, water levels at Shalufa are inversely correlated to the pressure at Dar Es-Salam. Hence, water level in the south reach of the canal is affected by waves created in the Indian Ocean due to atmospheric pressure variation.

The results of **Fig.24** show that relation between water level variation in the south reach of the canal (represented by water level at Shalufa and Port Tawfiq) and pressure over the Indian Ocean (represented by pressure at Dar Es-Salam) is good. From June, the water level at Temsah Lake approximated to the south reach of the cannal. The water levels of the south side were minimum value at summer, but the water levels of the north side were increased in July. The water level variation of Temsah Lake had good correspondence from January to June. The Temsah Lake locates middle of the Suez Canal. As the water level of the south side increase, the waves from the south side propagate to the Temsah Lake. These waves propagating are reached at Kantara in October.

6. Conclusions

Narrow passages between two large bodies of water are important hydraulic issue because of their navigational importance, typical hydrodynamic problems, and analysis difficulties. The present study concentrated on two important water passages: the Suez Canal, Egypt, and Kanmon Strait, Japan.

The study relied on numerical modelling using two dimensional, finite element model and field observation.

The study paid attention to two basic parts of the hydrodynamics of narrow passages: first, short term hydrodynamics influenced by tidal effect; second, long term hydrodynamic influenced by pressure variation.

From the short-term study, it was concluded that a wave propagating from one open sea is completely damped by the other sea. The damping causes a water-level gradient to develop within the narrow passage. The gradient is the direct cause of fast currents that usually threaten navigation within such passages.

From the long-term study, it is clear that atmospheric pressure variation has strong influence on long-term water-level variation.

The Suez Canal is divided by the Bitter and Temsah Lakes into three sections. The south-most section is similar to Kanmon Strait in its short-term behaviour. The north-most section is directly influenced by the pressure distribution prevailing on the Mediterranean Sea. The middle section receives propagations from the other two

sections. Both the tidal propagation in the north section and the atmospheric pressure influence on the south section need further considerations.

(Received on November 30, 1999)

References

1) Funk and Wagnalls Encyclopaedia: http://www.funkandwagnalls.com/encyclopaedia/
2) Nakazono: Kanmon Strait Arrangement, in *Sagyōsen,* no. 233, pp 50-53, September, 1997 (in Japanese)
3) Odamaki, M.: Co-Oscillating and Independent Tides of the Japan Sea, *Journal of Oceanographical Society of japan,* Vol.45, pp 217-232, 1989.
4) Murakami, M., Oonishi, Y., and Kunishi, H.: Heat and Salt Balance in the Seto Inland Sea, *Journal of Oceanographical Society of japan,* Vol.45, pp 204-216, 1989.
5) Hayakawa, N., Higo, T., Ueshima, H., Tanabe, H., Takasugi, Y., Fujiwara, T., Takarada, M., Yasada, H., Yuasa, I., Hashimoto, E., Yamazaki, M., and Yamada, M.: Studies of Tidal current and Dispersion by the Seto Inland Sea Hydraulic Model II, *Reports of the Government Industrial Research Institute, CHUGOKU,* No. 6, 92 pp, March, 1979.
6) Kashiyama, K., Ito, H., Behr, M, and Tezduyar, T.: Three-Step Explicit Finite Element Computation of Shallow Water Flows on a Massively Parallel Computer, *International Journal for Numerical Methods in Fluids,* Vol. 21,pp 885-900, 1995
7) Kashiyama, K., Saitoh, K., Behr, M., and Tezduyar, T.E.: Parallel Finite Element Methods for Large-Scale Computation of Storm Surges and Tidal Flows, *International Journal for Numerical Methods in Fluids,* Vol. 24, pp 1371-1389, 1997.
8) Kawahara, M., Hirano, H., Tsubota, K., and Inagaki, K.: Selective Lumping Finite Element Method for Shallow Water Flow, *International Journal for Numerical Methods in Fluids,* Vol. 2, pp 89-112, 1982.
9) Lorenzzetti, J.A., and Wang, J.D.: On the Use of Wave-Absorbing Layers in the Treatment of Open Boundaries in Numerical Coastal Circulation Models, *Applied Math. Modelling,* Vol. 10, pp 339-345, 1986.
10) Orlanski, I.: A Simple Boundary Condition for Unbounded Hyperbolic Flows, *J. Computational Physics,* Vol. 21, pp 251-269, 1976.
11) Chapman, D.C.: Numerical Treatment of Cross-Shelf Open Boundaries in a Barotropic Coastal Ocean Model, *J. Physical Oceanography,* Vol. 15, pp 1060-1075, 1985.
12) Bennett, A.F., and McIntosh, P.C.: Open Ocean Modelling as an Inverse Problem: Tidal Theory, *I. Phys. Oceanogr.,* Vol. 12, pp 1004-1018, 1982.
13) Koutitas, C., and O'Conner, B.: Modelling Three-Dimensional Wind-Induced Flows, *J. Hydr. Div., ASCE,* Vol. 106 (HY11), pp 1843-1865, 1980.
14) Kodama, T., Kawasaki, T., and Kawahara, M.: Finite Element Method for Shallow Water Equation Including Open Boundary Condition, *International Journal for Numerical Methods in Fluids,* Vol. 13, pp 939-953, 1991.
15) Elzeir, M., and Hibino, T.: Hydrodynamic Simulation of the Suez Canal; a Water Body Connecting Two Open Seas, *Annual Journal of Hydraulic Engineering, JSCE,* Vol. 43, pp 827-832, February, 1999.
16) Kodama, T., and Kawahara, M.: Multiple Level Finite Element Analysis for Tidal Current Flow with Non-Reflective Open Boundary Condition, *J. structural eng./earthquake eng., JSCE,* Vol. 9(1), No. 446/I-19, pp 89(77s)-99(87s), April, 1992.
17) Blumberg, A.F., and Kanta, L.H.: Open Boundary Condition for Circulation Models, *J. Hydr. Eng., ASCE,* Vol. 111(2), pp 237-255, 1985.
18) Elzeir, M., Tsuruya, H., and Hibino, H.: Hydrodynamic Simulation of Kanmon Strait; a Water Body

Connecting Two Open Seas, accepted, ICCE conference, Sydney, Australia, 2000.
19) Eid, F.M., Sharaf El-Din, S.H., and Alam El-Din, K.A.: Sea-Level Variation Along the Suez Canal, *Estuarine, Coastal, and Shelf Science,* Vol. 44, pp 613-619, 1997.
20) Hibino, T., Fukuoka, S., and Ikeuchi, K.: Characteristics of Internal Currents in Enclosed Brackish Lake with Seasonal and Daily Pressure Distribution Change, *Journal of Hydraulic, Coastal and Environmental Engineering, JSCE,* II-41, No. 579, pp 93-103, 1997 (in Japanese).
21) Hibino, T., and Tsuruya, H.: Correlation of Atmospheric Pressure Distribution and Sea Level for Japanese Coastal Waters: Consequence for an Estuary Environment, *J. Japan Soc. Hydrol. & Water Resour.,* Vol. 12, No. 2, pp 148-158, 1999.

List of Symbols

(1) Roman Symbols

A	wave amplitude (in the numerical experiment)
A_l	eddy viscosity
C	phase speed (in Sommerfeld OBC)
f	Coriolis force vector
f	Coriolis force component
g	gravitational acceleration
h	mean water depth
n	Manning coefficient
T_f	friction time scale in Blumberg and Kanta's OBC.
U	velocity vector
U	velocity component

(2) Greek Symbols

Δt	time increment for finite element discretization
ζ	water level variation with respect to mean water level.
τ	bottom friction
φ	dummy to indicate any variable
ω	wave frequency

(3) Subscripts and Superscripts

i, j, k	indices indicating spatial dimensions of the discretized variables
x	derivative with respect to x
n	value normal to the open boundary
I	incident wave

(4) Abbreviations

ADCP	Acoustic Doppler Current Profiler
FEM:	Finite Element Method
HWL	High Water Level
LWL:	Low Water Level
MWL:	Mean Water Level
NNS	Nihowan-Nakaumi-Shinjiko domain
OBC:	Open Boundary Condition